1040-5488/14/9107-0713/0 VOL. 91, NO. 7, PP. 713–722
OPTOMETRY AND VISION SCIENCE

ORIGINAL ARTICLE

The Bigaussian Nature of Ocular Biometry

Jos J. Rozema* and Marie-José Tassignon†; for EVICR.net, Project Gullstrand Study Group

ABSTRACT

Purpose. To study how the leptokurtic shape of the refractive distribution can be derived from ocular biometry by means of a multivariate Gaussian model.

Methods. Autorefraction and optical biometry data (Scheimpflug and partial coherence interferometry) were obtained for 1136 right eyes of healthy white subjects recruited by various European ophthalmological centers participating in Project Gullstrand. These biometric data were fitted with linear combinations of multivariate Gaussians to create a Monte Carlo simulation of the biometry, from which the corresponding refraction was calculated. These simulated data were then compared with the original data by histogram analysis.

Results. The distribution of the ocular refraction more closely resembled a bigaussian than a single Gaussian function (F test, $p < 0.001$). This also applied to the axial length, which caused the combined biometry data to be better represented by a linear combination of two multivariate Gaussians rather than by a single one (F test, $p < 0.001$). Corneal curvature, anterior chamber depth, and lens power, on the other hand, displayed a normal distribution. All distributions were found to gradually change with age. The statistical descriptors of these two subgroups were compared and found to differ significantly in average and SD for the refraction, axial length, and anterior chamber depth. All distributions were also found to change significantly with age.

Conclusions. The bigaussian model provides a more accurate description of the data from the original refractive distribution and suggests that the general population may be composed of two separate subgroups with different biometric properties. (Optom Vis Sci 2014;91:713–722)

Key Words: ocular refraction, statistical eye model, ocular biometry, myopia, hyperopia

Like most other human physical traits, ocular dimensions tend to occur in a large population according to Gaussian distributions.[1–5] The distribution of the axial length, however, resembles a Gaussian that is skewed toward longer values in some populations. The measured biometric parameters combine to an ocular refraction value that is either close to 0 diopters (D), indicating optical balance (emmetropia), or significantly different from 0 D, indicating an optical imbalance (ametropia). Given that almost all biometric parameters follow a Gaussian distribution, it would be expected that the resulting refraction would be similarly distributed. However, in practice, the prevalence of the ocular refraction is too leptokurtic for a Gaussian distribution, with a sharp central peak and long tails.[6–12] This is often taken as proof of emmetropization, a process that fine-tunes the ocular components toward emmetropia during childhood, thus creating a higher-than-expected proportion of emmetropes in the general population.

In an attempt to explain the leptokurtic shape of the refractive distribution, Sorsby[5] suggested that the emmetropic peak may be the result of strong correlations between ocular parameters. Using a statistical eye model and his 1957 data set,[3] he demonstrated that a lack of correlations between ocular parameters would result in a very broad distribution, whereas nonzero correlation values would lead to a distribution that was considerably narrower. Although mathematically correct, Sorsby's numeric model used an incorrect value for the correlation between the keratometry and axial length (-0.877 instead of the correct value of -0.293) that caused him to find a Gaussian peak that was too sharp (SD of 1.56 D instead of 3.51 D). Hence, the correlation between all combinations of biometric parameters cannot provide sufficient explanation for the narrow shape of the emmetropic peak.

In a recent publication, Flitcroft[13] proposed that, rather than considering the refractive distribution as a single Gaussian distribution, one could consider it as a sum of two subpopulations, called "emmetropized" and "dysregulated." Flitcroft postulated that the

*PhD
†MD, PhD
Department of Ophthalmology, Antwerp University Hospital, Edegem, Belgium (both authors); and Department of Medicine and Health Sciences, Antwerp University, Wilrijk, Belgium (both authors).

Supplemental digital content is available for this article. Direct URL citations appear in the printed text and are provided in the HTML and PDF versions of this article on the journal s Web site (www.optvissci.com).

main distinction between both subpopulations was the successfulness of the emmetropization process during childhood, resulting in a sharp peak centered at 0 D corresponding with individuals for whom this process was successful, and a second, much broader peak with individuals that either had a very limited degree of emmetropization or had a degree of myopization. The proposed model, involving a sum of two Gaussians, provides a much closer fit of the refraction distribution than a monomodal model.[13] In a follow-up article, Flitcroft[14] subsequently proposed a descriptive model for the refractive development based on parameters such as myopic onset, myopic progression biological noise, genetic bias, and so on, which were inserted in a Monte Carlo simulation. This simulation was found to give a realistic description of the changes in the refractive distribution for subjects aged 3 months to 24 years. It does not, however, look at how the ocular refraction results from the ocular biometry.

The goal of this article is to expand on Flitcroft's emmetropization hypotheses to include biometry and to study how ocular parameters that generally have Gaussian distributions lead to a leptokurtic refractive distribution. This is done using a Monte Carlo simulation of multivariate Gaussian model,[5,15] after an analysis of the number of Gaussian functions required for an accurate description of the biometric data. Based on this model, an analysis of the influence of age on the refraction distribution was performed on a large cohort.

METHODS

Subjects

This work used the binocular biometric data of 1136 randomly selected eyes of 1136 healthy white subjects (487 men, 649 women) aged between 20 and 70 years and with a spherical equivalent refraction ranging from −10 to +10 D. Subjects were recruited in urban and suburban areas near the participating sites, spread all over Europe (Germany: 2 sites, 408 subjects; Belgium: 1 site, 184 subjects; Spain: 4 sites, 283 subjects; Israel: 1 site, 188 subjects; Italy: 3 sites, 66 subjects; Portugal: 1 site, 7 subjects). Exclusion criteria were previous ocular pathology or surgery, an intraocular pressure higher than 22 mm Hg, wearing hard contact lenses less than 1 month before testing, and pregnancy. The data used in this work were collected in Project Gullstrand, a European multicenter study organized through EVICR.net with the aim of determining the correlation between ocular biometry and several psychophysical tests. The study adhered to the tenets of the Declaration of Helsinki and received approval from the ethics committee of the Antwerp University Hospital (Ref. B300200724O6). Signed informed consent was obtained from all participating subjects before testing.

Subjects were not cyclopleged before the measurements to remain as close as possible to the everyday physiological conditions of the eye. This may have somewhat increased the prevalence of myopia in some eyes.

Materials

The biometric equipment used in the different sites consisted of an autorefractometer (various types) for objective spherical equivalent refraction SE, a Scheimpflug camera (Pentacam, Oculus Optikgeräte, Wetzlar, Germany; Galilei, Ziemer Ophthalmic Systems, Port, Switzerland; Sirius, CSO, Scandicci, Italy) for the average anterior keratometry K, and the total anterior chamber depth ACD (i.e., from corneal epithelium to the anterior lens surface). An ocular biometer provided measures for the axial length L (IOL Master, Carl Zeiss, Jena, Germany, or Lenstar, Haag-Streit, Koeniz, Switzerland). From these data, the crystalline lens power P_L was estimated using the Bennett-Rabbetts method with optimized constants[16] and the whole eye power P_{eye} was derived from Gullstrand's thick lens equation assuming a refractive index $n = 1.336$ for the humors and a distance between the corneal apex and the first lenticular principal point of ACD + 3.1 mm.

Because the instruments used in this work are not uniform across the measuring centers, one should verify whether the measurements provided by these devices are all comparable. Many articles have been published in the literature on this subject,[17–23] some of which reporting equivalence between devices and many others reporting significant differences. For this reason, the intraclass correlation (ICC) between sites was calculated to estimate the influence of between-site differences in equipment.

Multimodal Gaussian Fit

The bigaussian refractive distribution reported by Flitcroft[13] was verified by fitting the refractive distribution with a linear combination of M Gaussians:

$$f(\mathrm{SE}) = \sum_{i-1}^{M} \frac{a_i}{\sqrt{2\pi}} \exp\left(-\frac{(\mathrm{SE} - b_i)^2}{2c_i^2}\right) \quad (1)$$

where a_i are the amplitudes of the Gaussian modes, b_i (in diopters) are the locations of the peaks, and c_i (in diopters) are the SDs. In case of a normalized distribution (i.e., surface under the curve equals unity), the amplitudes are related by $\sum_i a_i = 1$.

To study how the refractive distribution results from the ocular biometry, the prevalence of the keratometry K, anterior chamber depth ACD, lens power P_L, and axial length L were modeled using a linear combination of M multivariate Gaussians:

$$f(x) = \sum_{i-1}^{M} \frac{1}{\sqrt{(2\pi)^4 |C_i|}} \exp\left(-\frac{1}{2}(x - B_i)' C_i^{-1} (x - B_i)\right) \quad (2)$$

where B_i is a (1 by 4) vector describing the mean values of the biometric parameters and C_i is a (4 by 4) matrix containing the covariance values between these parameters. The values for B_i and C_i were estimated using Gaussian mixture models, an implementation of the Expectation-Maximization (EM) algorithm devised specifically for fitting multivariate Gaussian functions. This algorithm is an iterative process that uses an initial estimate based on a random sample of the original data points. Depending on the number of available data points, this may cause the result of the multivariate Gaussian fits to vary somewhat between runs.

Once a multivariate Gaussian model was determined, it was used in a Monte Carlo procedure to generate a large, synthetic data set that is distributed according to the model. For these generated data points, the corresponding refraction was derived using the Bennett-Rabbetts equation,[24] with the anterior principal point of

the lens located at 3.04 mm behind the lens apex. The distribution of this calculated refraction is then compared with that of the measured refraction as a verification of the model.

Statistics

All statistics were calculated using MS Excel 2010 (Microsoft, Redmond, WA) and Matlab R2011b (The MathWorks, Natick, MA).

RESULTS

Between-Site Effects

This work uses biometric data from various sites, with minor differences in average age, sex balance, and equipment, each of which may influence the results presented. For this reason, the ICCs were calculated in an effort to estimate the importance of these between-site differences. These were found to be very small for all parameters (ICC < 0.10), both for differences in average values as in SD. Hence, a correction for site-specific effects was deemed unnecessary.

Fitting the Refractive Distribution

Like most reports in the literature, the distribution of the spherical equivalent refraction in our data was not normally distributed (Komolgorov-Smirnov test, $p < 0.001$), with an excess kurtosis of 1.794 (i.e., leptokurtic) and a skewness of −0.763 (i.e., moderately skewed toward myopia). Although the coefficient of determination was high ($r^2 = 0.935$, $p < 0.001$), a Gaussian fit did not give a good fit of the myopic and hyperopic tails, or of

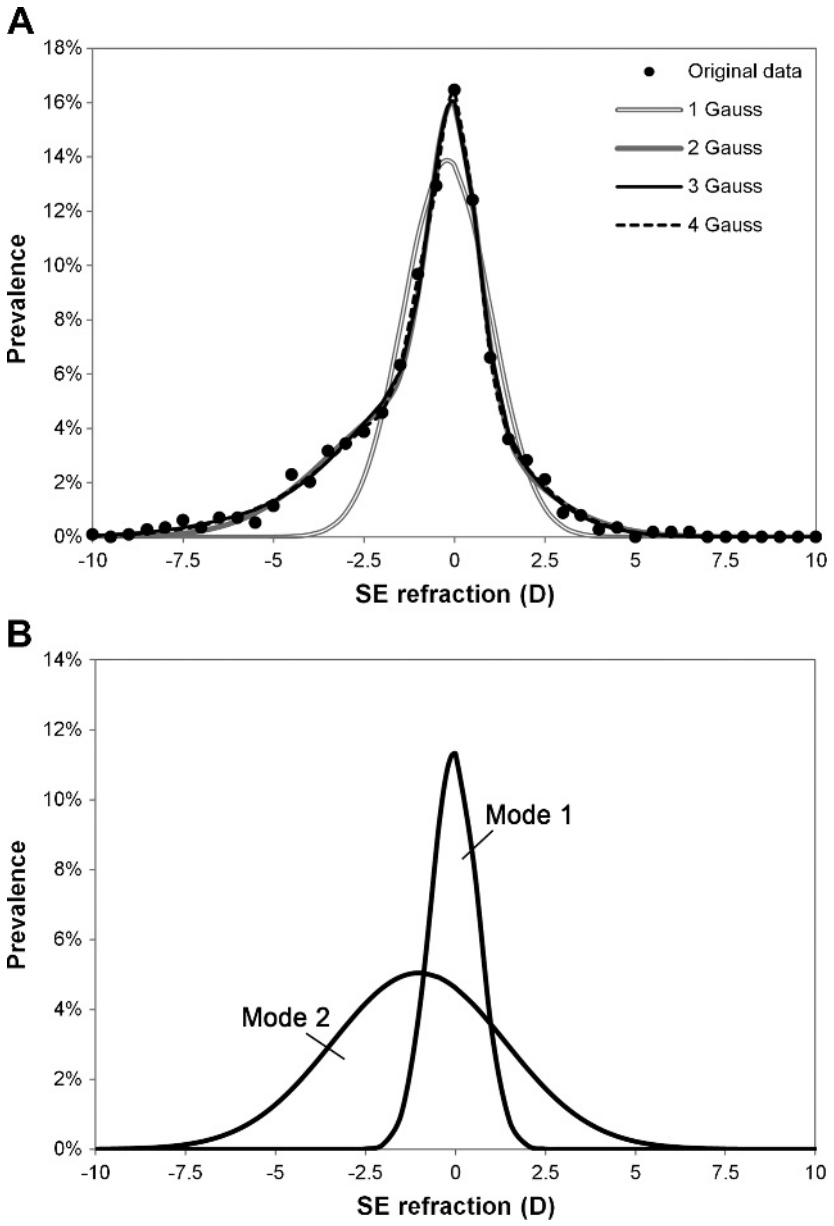

FIGURE 1.

(A) Distribution of the refraction, fitted by a single Gaussian function and linear combinations of two, three, or four Gaussian functions. (B) Refraction of the individual modes of the bigaussian model.

the emmetropic peak (Fig. 1A). By fitting a sum of two Gaussians to the refractive distribution, both the emmetropic peak and the ametropic tails were included into the model (Fig. 1B), which improved the coefficient of determination to $r^2 = 0.994$ ($p < 0.001$). Including a third or fourth Gaussian on the other hand, however, did not significantly improve the fit, with r^2 values of 0.995 ($p < 0.001$) and 0.998 ($p < 0.001$), respectively. Applying an F test on the squared difference between the measured data and the model predictions for each consecutive Gaussian model resulted in a significant difference between the one- and two-Gaussian models ($p < 0.001$) but not between the two- and three-Gaussian models ($p = 0.756$). As the differences in the graph are almost indistinguishable for the latter two models, it is safe to conclude that a linear combination of only two Gaussians can reliably describe the refractive distribution.

Fitting the Biometric Data with a Multivariate Model

To derive how the refractive distribution from Fig. 1 originates from the distributions of the biometric parameters K, ACD, P_L, and L, the EM algorithm was used to fit a linear combination of up to 6 four-dimensional multivariate Gaussians to the 1136 available data points. The distributions predicted by the fitted models were averaged over 100 runs and compared with those of the original measurements to determine the most suitable description.

As is seen in Fig. 2, the distributions of K, ACD, and P_L predicted by a single multivariate Gaussian corresponded well with those of the original distribution. This was also seen from their coefficients of determination r^2, which did not change significantly when more Gaussians were added (F test applied to the squared differences between measured and modeled values: $p > 0.05$; Table 1). For axial length L, a sum of two Gaussians

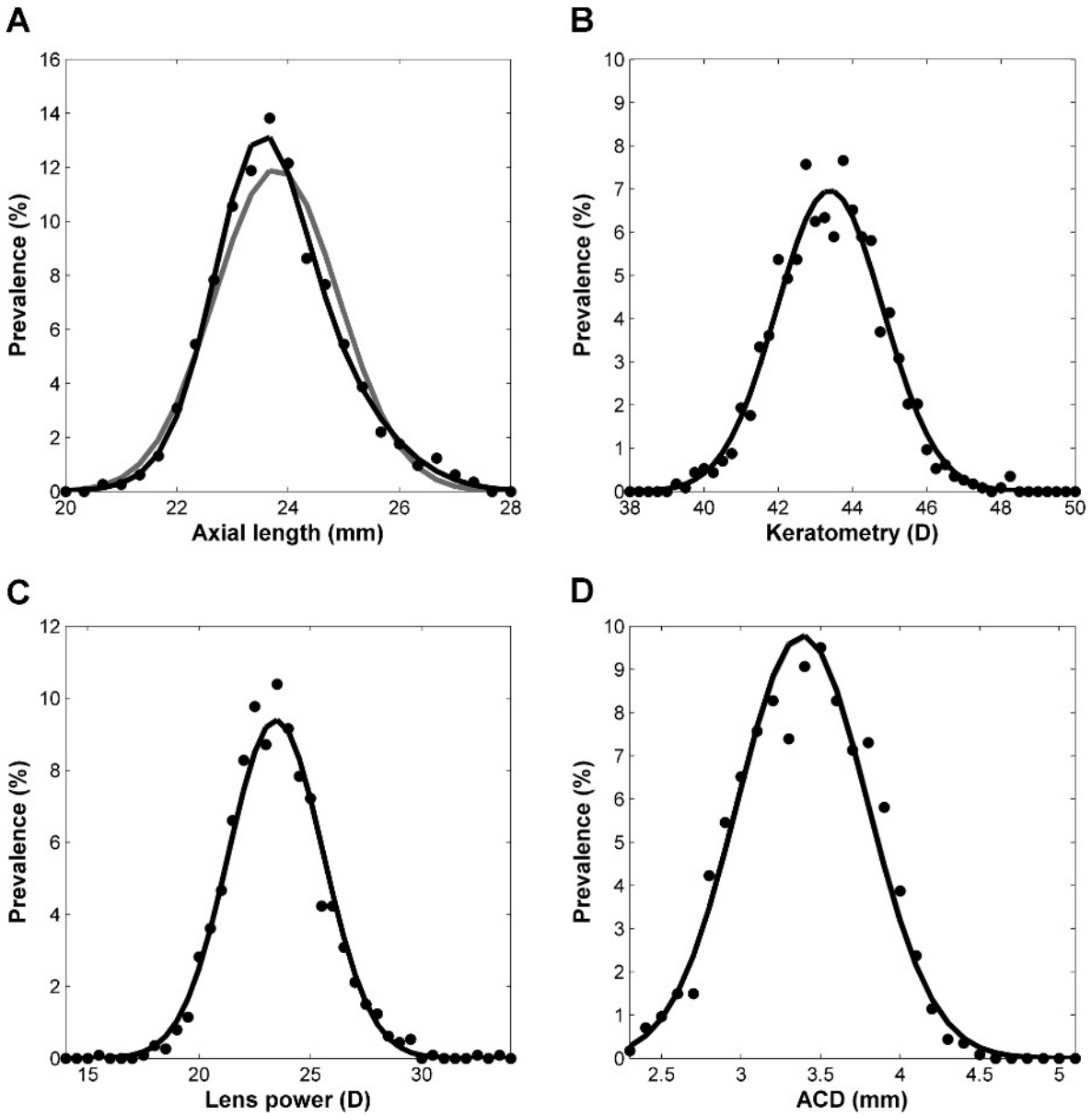

FIGURE 2.

Comparison of the original distributions (black markers) and distributions predicted by one multivariate Gaussian (gray lines), or a linear combination of two multivariate Gaussians (black line) for (A) axial length, (B) keratometry, (C) lens power, and (D) anterior chamber depth.

TABLE 1.

Change in the coefficient of determination for various measured parameters in comparison with model predictions (average over 100 runs)

	No. multivariate Gaussians					
Histogram frequency	1	2	3	4	5	6
K	0.974*	0.974	0.974	0.973	0.973	0.973
ACD	0.899*	0.899	0.899	0.917	0.916	0.918
P_L	0.981*	0.981	0.982	0.981	0.984	0.978
L	0.963	0.992*	0.991	0.990	0.989	0.989
K vs. *L*	0.743	0.804*	0.804	0.803	0.804	0.804
P_L vs. *L*	0.843	0.872*	0.872	0.872	0.871	0.872
ACD vs. *L*	0.784	0.813*	0.819	0.819	0.820	0.820
P_L vs. *K*	0.772*	0.772	0.779	0.780	0.781	0.781
ACD vs. *K*	0.737*	0.737	0.741	0.744	0.745	0.746
P_L vs. ACD	0.793	0.794	0.810*	0.812	0.813	0.815
SE (calc. vs. meas.)	0.778	0.982*	0.986	0.990	0.992	0.993

Calc. vs. meas., SE calculated from simulated biometry versus measured biometry.

*Significant difference from preceding model (F test on the squared difference with original data; significant at $p < 0.05/55 = 0.000909$ after Bonferroni correction for 55 comparisons).

was found to give a significantly better fit than a single Gaussian (F test, $p < 0.001$). Linear combinations of more than two Gaussians did not improve this result.

Fig. 3 shows the correlations between various biometric parameters for the original data (gray markers) and the model predictions using one, two, and three multivariate Gaussians (black contours). Overall, the contours of the two-Gaussian model followed the distribution of the original data points well, indicating that the originally measured data and the generated data were similar. Comparing the squared differences between the 2D histograms for the original data and the model predictions using an F test, the correlations involving the axial length (i.e., *K* vs. *L*, P_L vs. *L*, and ACD vs. *L*) were significantly better described by two multivariate Gaussians, whereas P_L vs. ACD was best described by three multivariate Gaussians (Table 1). For the other correlations (*K* vs. P_L and *K* vs. ACD) a single multivariate Gaussian was sufficient.

Lastly, the corresponding refractive distributions were derived by performing Monte Carlo simulations based on the multivariate Gaussian fits, followed by the Bennett-Rabbets equation. As is seen in Fig. 4, the refractive distribution for a single Gaussian does

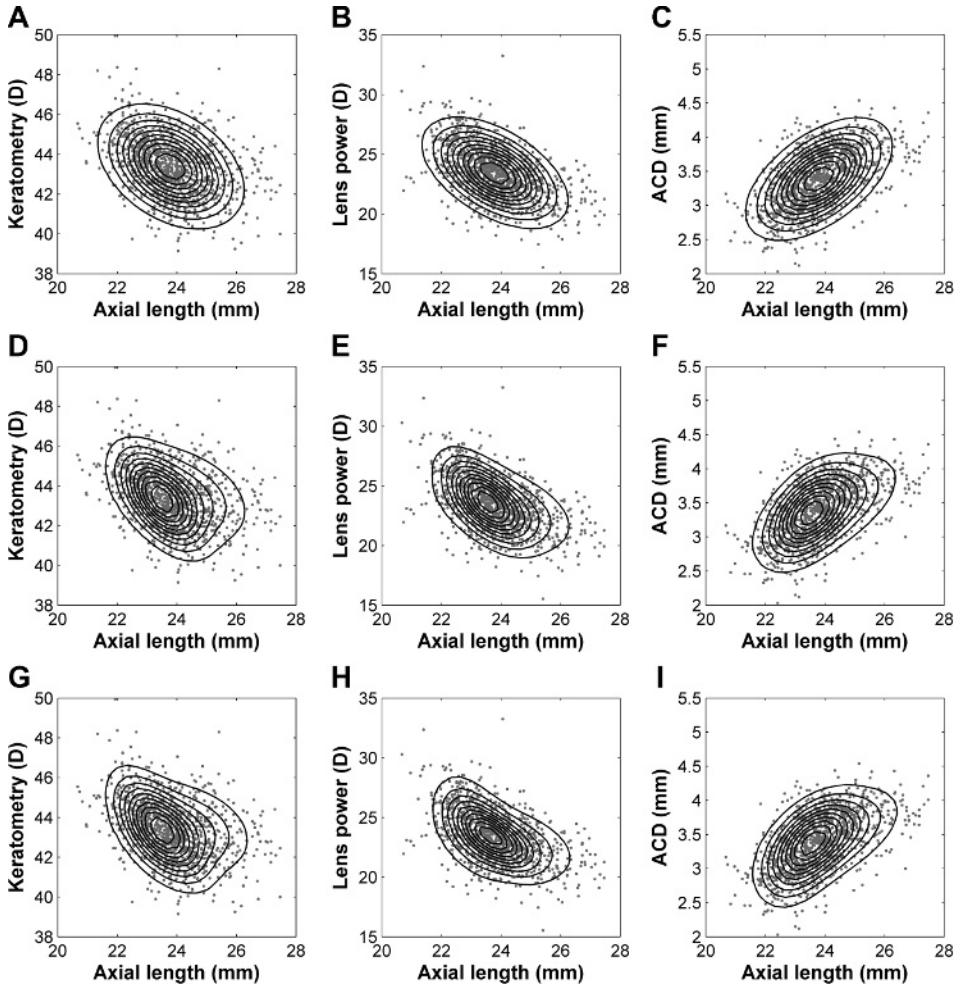

FIGURE 3.

Comparison of the original distribution (gray markers) and the distributions predicted by one multivariate Gaussian (A, B, C), or a linear combination of two (D, E, F) or three multivariate Gaussians (G, H, I) for the correlations between keratometry and axial length (A, D, G), lens power and axial length (B, E, H), and anterior chamber depth and axial length (C, F, I).

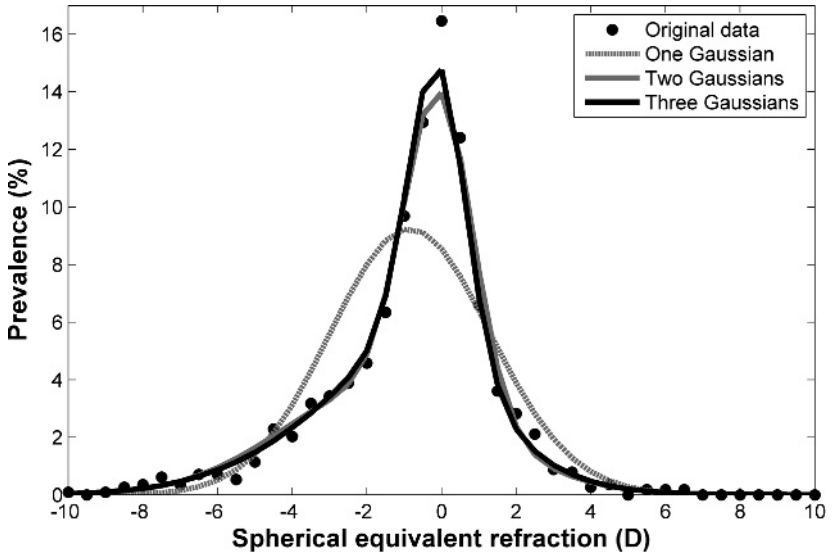

FIGURE 4.

Comparison of the original refractive distribution (black markers) and the distributions corresponding with one multivariate Gaussian (dashed gray line), or a linear combination of two (solid gray line) or three (black line) multivariate Gaussians. These graphs represent the average distribution over 100 runs of the EM algorithm.

not correspond very well with the original distribution of the refraction. This improved significantly for a linear combination of two multivariate Gaussians (F test, $p < 0.001$; Table 1), but no further for three or four Gaussians (F test, $p > 0.001$).

In summary, we found that a single multivariate Gaussian can accurately describe 5 of the 11 histograms considered, whereas a linear combination of two Gaussians was necessary for 5 of the 11 histograms (4 of which involved the axial length *L*), and only one case required a sum of three Gaussians. The fit parameters for three or four Gaussians were found to vary considerably between runs, however, as the random sampling required to make an initial estimate caused overfitting of random fluctuations in the original data (see Appendix figure, available at http://links.lww.com/OPX/A176). Based on these observations, we concluded that a fit of two multivariate Gaussians suffices for a description of the relationship between biometry and refraction and avoids overfitting of the data.

Comparison of the Modes in the Bigaussian Model

The shape of the contours in Fig. 3D to F is the sum of two sets of ellipses, corresponding with the two multivariate Gaussians modes (henceforth referred to as modes 1 and 2). Both sets of ellipses differ from each other in centration, size, and orientation, corresponding with the mean, SD, and regression slope, respectively (Table 2). Comparing the mean parameter values of the two modes by means of an unpaired *t* test, significant differences were found for all parameters studied (i.e., SE, *K*, ACD, P_L, and *L*). Subsequent Levene tests also confirmed significant differences in SD for SE and *L*. Finally, the regression slopes of SE versus ACD, SE versus P_L, *L* versus *K*, *L* versus P_L, *L* versus ACD, and P_L versus ACD were significantly different between modes (regression analysis with interaction term; $p < 0.001$).

These results suggest that multivariate mode 1, corresponding with the emmetropic peak of the refractive distribution, has, on

TABLE 2.

Statistical descriptors of modes 1 and 2 of the bimodal multivariate model (B_i and C_i matrices in equation 2 averaged over 100 runs of the algorithm)

			Pearson correlation (*r*)					
	Symbol, unit	Mean (SD)	*K*	ACD	P_L	*L*	*t* test*	Levene test*
Mode 1	SE, D	−0.15 (0.97)	−0.06	−4.01	−0.187	−0.319	<0.001†	<0.001†
	K, D	43.30 (1.44)	—	0.048	0.086	−0.615	<0.001†	0.451
	ACD, mm	3.33 (0.40)		—	−0.193	0.199	<0.001†	0.069
	P_L, D	23.82 (2.09)			—	−0.598	<0.001†	0.092
	L, mm	23.41 (0.81)				—	<0.001†	<0.001†
Mode 2	SE, D	−1.56 (2.79)	−0.072	−0.504	−0.031	−0.805		
	K, D	43.48 (1.42)	—	0.064	0.002	−0.311		
	ACD, mm	3.45 (0.41)		—	−0.082	0.348		
	P_L, D	22.52 (2.08)			—	−0.370		
	L, mm	24.21 (1.26)				—		

*Comparison of the biometric parameters of modes 1 and 2.

†Significant differences at a significance level of $p < 0.05/5 = 0.001$ (Bonferroni correction for five comparisons).

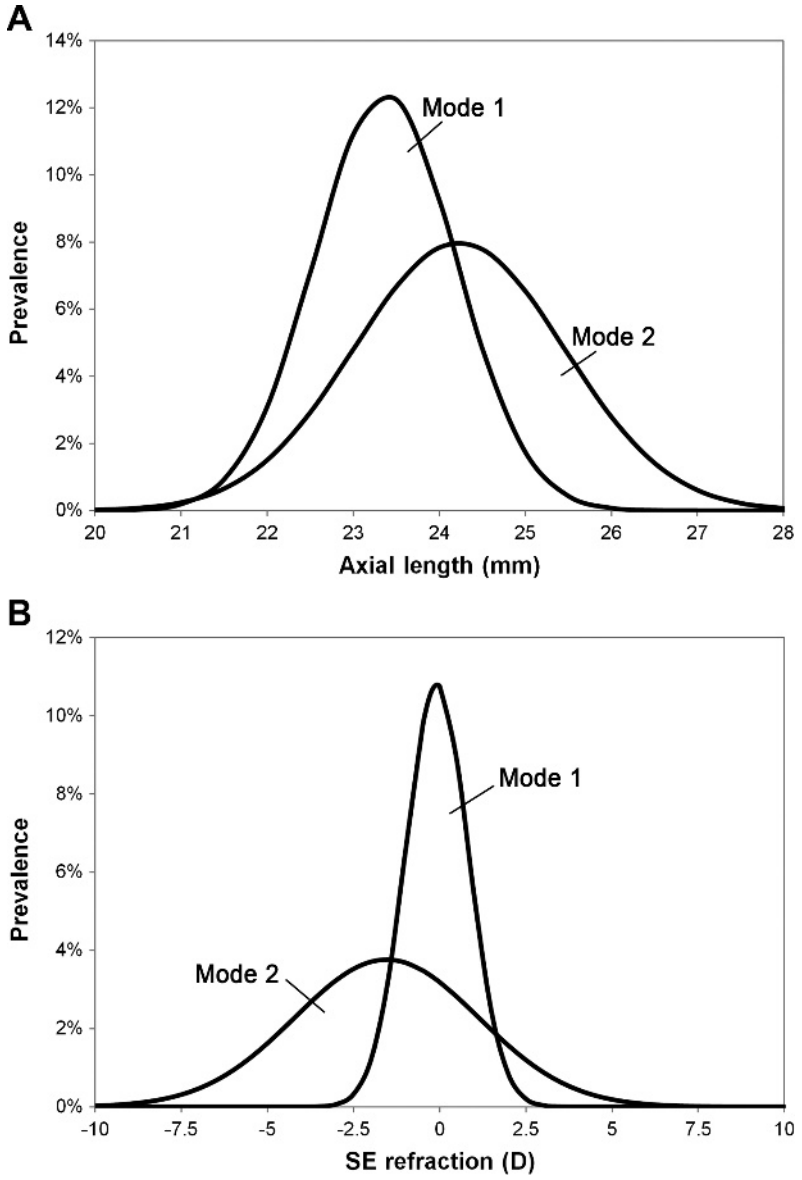

FIGURE 5.
Bigaussian multivariate model split up in individual modes for (A) axial length and (B) refraction.

average, significantly shorter eyes, flatter corneas, shallower ACD, and a higher lens power than multivariate mode 2. The proportions of both modes is 49–51% for modes 1 and 2, respectively. This is also shown in Fig. 5, where the individual contributions of modes 1 and 2 are shown for axial length and SE refraction.

Influence of Age

From the literature, it is known that ocular biometry changes considerably with age, which would also influence the results described above. The analysis was therefore repeated for subgroups of the study cohort defined by decade of age. Table 3 illustrates that there are significant variations with age for almost all parameters studied, with a near monotonous decrease in ACD and in P_L in both modes. This causes the peaks of modes 1 and 2 to undergo a significant hyperopic shift with age (analysis of variance; $p < 0.001$; Fig. 6).The hyperopic shift of the mode 2 peak occurs faster than for the mode 1 peak, causing both peaks to move closer to each other with age (see refraction values in Table 3).

DISCUSSION

Flitcroft[13] originally proposed that the refractive distribution of normal eyes could be described well by the sum of two Gaussian functions, corresponding with an emmetropic peak around 0 D superimposed on a much broader distribution (Fig. 1). The results presented in this study confirm this proposition. This raises the question of whether these modes represent actual subgroups of the general population or are merely mathematical constructs.

We can address this by considering Flitcroft's refraction model,[14] which gives the refractive development during childhood in individual eyes. Using this model and a Monte Carlo process, he was able to show how the refractive distribution changes from a Gaussian centered at light hypermetropia at birth to emmetropia at the age of 2 to 3 years. The emmetropization process, however,

TABLE 3.

Comparison of the simulated ocular biometry in modes 1 and 2 per age group (B_i and C_i matrices in equation 2 averaged over 100 runs of the algorithm)

	Parameter, unit	Mean (SD) per age group					ANOVA*
		20–30 y	30–40 y	40–50 y	50–60 y	60–70 y	
	Total no. eyes	236	270	232	233	166	
	% Mode 1	61.7	52.5	62.9	61.0	66.2	—
	% Mode 2	38.3	47.5	37.1	39.0	33.8	—
Mode 1	SE, D	−0.68 (1.36)	−0.27 (1.07)	−0.31 (1.42)	0.29 (1.52)	0.87 (1.80)	<0.001*
	K, D	43.49 (2.87)	43.08 (1.93)	43.28 (2.00)	43.52 (2.20)	43.52 (1.83)	0.111
	ACD, mm	3.63 (0.12)	3.38 (0.13)	3.28 (0.14)	3.17 (0.12)	3.09 (0.10)	<0.001*
	P_L, D	24.51 (4.59)	24.48 (4.13)	23.55 (3.63)	23.03 (3.40)	22.02 (3.04)	<0.001*
	L, mm	23.56 (0.85)	23.40 (0.62)	23.50 (0.59)	23.30 (0.70)	23.27 (0.55)	<0.001*
Mode 2	SE, D	−2.80 (2.96)	−2.27 (3.74)	−1.80 (4.05)	−1.06 (4.09)	−1.09 (3.19)	<0.001*
	K, D	43.59 (1.03)	43.45 (2.00)	43.11 (1.68)	43.42 (2.08)	43.57 (2.16)	0.041
	ACD, mm	3.78 (0.08)	3.59 (0.08)	3.40 (0.13)	3.26 (0.17)	3.27 (0.20)	<0.001*
	P_L, D	23.47 (3.10)	22.96 (2.65)	22.87 (4.55)	21.50 (3.46)	21.36 (5.16)	<0.001*
	L, mm	24.58 (1.09)	24.44 (1.48)	24.28 (1.77)	24.17 (1.94)	24.34 (1.26)	0.049

*Calculated from summary data. Significant differences at a significance level of $p < 0.05/10 = 0.005$ (Bonferroni correction for 10 comparisons).

ANOVA, analysis of variance.

is not equally effective for all individuals. Some people that are born ametropic are able to emmetropize over several diopters, whereas for others the refraction barely changes, leaving them close to their initial refraction. However, even if the emmetropization process is not optimal in the latter group, one may still find a large number of "lucky" dysregulated emmetropes that were born with a refraction close to emmetropia and hence did not require much emmetropization to begin with. Later, after the age of 6 to 7 years, a second dysregulation occurs in some individuals in the form of myopia. This causes a gradually increasing skewness on the myopic side of the refractive distribution and has been associated with a large variety of factors.[25] All of these effects combined lead to a bigaussian distribution of the refraction, with a sharp mode attributed to the emmetropization process ("emmetropized"), superimposed over a much broader mode associated with dysregulation (poor emmetropizers, some of which are emmetropic by chance, and myopes). As such, the analysis of this bigaussian description goes deeper than common descriptive statistics and may therefore be useful in epidemiological studies.

Because refraction results from a combination of ocular biometric parameters, we took Flitcroft's model one step further in this work and studied how the bigaussian nature of the refraction can be derived from the biometry of adult eyes. For this, we used a multivariate Gaussian model of the ocular biometry as a

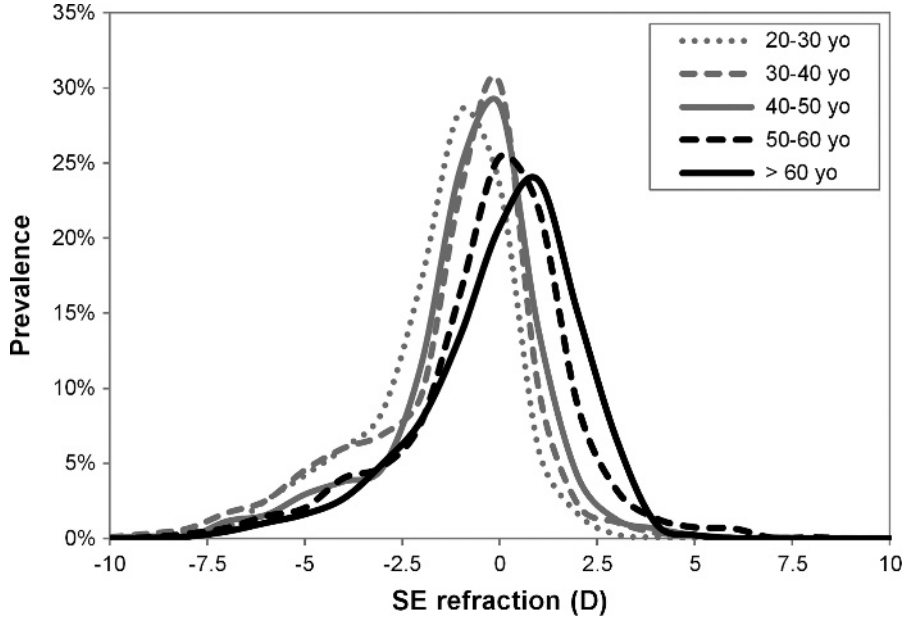

FIGURE 6.

Changes in the bigaussian model with age.

base for Monte Carlo simulations. This approach also allowed a calculation of the associated refractive distribution for comparison with the measured refractive distribution as a means of verifying the results.

The first step determined how many multivariate Gaussians were required to accurately represent the four-dimensional data given by keratometry K, anterior chamber depth ACD, crystalline lens power P_L, and axial length L. This was determined using the histograms of the four individual parameters (Fig. 2), as well as the two-dimensional histograms based on the scatter plots describing the correlations between parameters (Fig. 3). For this, the distributions associated with the axial length L were found to be skewed and better described by the bigaussian model (Table 1). This, however, did not apply to the keratometry K, anterior chamber depth ACD, and crystalline lens power P_L, for which a monomodal model was sufficient. These results confirm that, because axial length is known to be the main source of myopia,[26] the bigaussian nature of the refractive distribution can be mostly attributed to the bigaussian nature of the distribution of L.

The sum of two multivariate Gaussian modes, however, was not able to fully reproduce the entire height of the emmetropic peak in the refractive distribution (Fig. 4). This discrepancy could result from nonlinear effects, such as higher-order correlations between parameters that are not included into the current model. For this reason, we opted to use a bigaussian model for further analysis.

Comparing the two multivariate Gaussian modes, we found significant differences in mean values for all parameters (SE, K, ACD, P_L, and L) and in the SDs of SE, ACD, and L. For the most part, these differences reflect known differences between emmetropes and myopes, such as steeper corneal curvatures,[27,28] deeper anterior chambers,[29] lower crystalline lens powers,[30] and longer axial lengths[21] for myopes. However, there were also differences that have not been mentioned before in the literature, such as the significant differences between modes in regression slopes of SE versus ACD, SE versus P_L, L versus K, L versus P_L, L versus ACD, and P_L versus ACD. The first five may be the result of a difference in range for SE between modes (with the SE range of mode 2 being three times that of mode 1). The difference in P_L versus ACD, on the other hand, might point at something more fundamental that may deserve some further investigation in the future.

The shape of the refractive distributions is influenced by the subject's age, or rather a combination of age and time because the data set is not longitudinal. When the data were subdivided per decade of age, a significant hyperopic shift was seen in both modes (Fig. 6, Table 3). This shift occurs somewhat faster in the ametropic mode 2 than in the emmetropic mode 1, making the mode 2 peak more distinct in younger eyes than in older eyes. This is most likely an expression of the increased prevalence of myopia in young people over the past few decades. This is also seen in the weight of the ametropic mode 2, which, on average, is more important for subjects younger than 40 years than for subjects older than 40 (Table 3). Besides these observations, the known age-related changes of the eye are seen, such as a hyperopic shift in refraction and a decrease in P_L and a decrease in ACD.

In an attempt to simplify the model, we also attempted to use an alternative description, involving a single multivariate Gaussian after a Box-Cox transformation of L. This led to a better fit of L compared with a single, untransformed Gaussian (r^2 = 0.989 and 0.963, respectively; F test: $p < 0.001$) but not as good as a bigaussian (r^2 = 0.989 and 0.992, respectively; F test: $p = 0.002$). For the calculated SE, there was no significant improvement from transforming L in the multivariate Gaussian (r^2 = 0.827 and 0.778 for transformed and not transformed, respectively; F test: $p = 0.194$), and the resulting distribution looked much like that of the untransformed Gaussian. Therefore, power transformation was not considered a viable option for our purposes.

Note that although the data were collected across different locations with varying equipment, the influence of these differences was found to be negligible (ICC < 0.10). We therefore feel comfortable that this had only a minimal effect on our results.

In conclusion, this study further describes the bigaussian nature of refraction initially described by Flitcroft but expands it to also apply to ocular biometry. This is the first time that the model was validated prospectively in normal volunteers and that the bigaussian distribution of refraction was reproduced. In addition, the possibility that the refractive distribution is better described by more than two Gaussian curves was examined and discounted. This bigaussian nature was also confirmed for axial length, whereas corneal curvature, anterior chamber depth, and lens power are still best described by a normal distribution. These findings not only support the bigaussian nature of refraction but also confirm that emmetropized and dysregulated eyes have on average a different ocular biometry, although a large degree of overlap exists between both groups. Further investigation is required to understand why these groups exist apart from one another and what factors account for the divergence at an early age.

ACKNOWLEDGMENTS

Project Gullstrand Study Group

Study Sponsor

EVICR.net—European Vision Institute Clinical Research Network, AIBILI, Azinhaga de Santa Comba, Celas, 3000-548 Coimbra, Portugal.

Coordinating Investigator

Jos J. Rozema.

Coordinating Center

EVICR.net.

Data Collection by EVICR.net Clinical Sites (CS)

CS 02—Mainz (Germany): Katrin Lorenz and Mascha von Trentini; CS 07—Alicante (Spain): Espranza Sala Pomares, Maria José Garcia Corral, Laurent Bataille, and Jorge L. Alió; CS 12—Antwerp (Belgium): Jos J. Rozema, Sien Jongenelen, Irene Ruiz-Hidalgo, and Marie-José Tassignon; CS 27—Leipzig (Germany): Franziska Georgia Rauscher, Maria Teresa Blüsch, Jens Dawczynski, and Peter Wiedemann; CS 36—Rome (Italy): Luigi Mosca, Laura Guccione, Monica Riso, Maria Emanuela Toro, and Alessandra Rosati; CS 38—Barcelona (Spain): Francesco Duch, Raimon Escude, Alexia Martinez, and Antonio Morilla-Grasa; CS 51—Valencia (Spain): Cristina Peris-Martínez, Amparo Díez Ajenjo, and Carmen Garcia Domene; CS 51—Girona (Spain): Maria Bozal De Febrer, Teresa Torrent Solans, and Alicia Verdugo Gazdik; CS 60—Tel Aviv (Israel): David Varssano and Barbara Gold; CS 63—Chieti (Italy): Lisa Toto, Alessandra Mastropasqua, and Leonardo Mastropasqua; CS 67—Milan (Italy): Francesco Fasce, Alessandra Spinelli, Karl Knutsson, and Giovanni Fogliato.

The authors thank Kristien Wouters, Frank Schaeffel, and Ian Flitcroft for discussions that helped us to improve this article.

This project was supported in part by a research grant from the Flemish government agency for Innovation by Science and Technology (grant nr IWT/110684). The authors declare no competing interests.

Received October 1, 2013; accepted May 2, 2014.

APPENDIX

The appendix, a figure showing the distribution of the calculated refraction associated with the individual multivariate Gaussian modes for 100 consecutive runs of the algorithm, is available at http://links.lww.com/OPX/A176.

REFERENCES

1. Tron E. Über die optischen Grundlagen der Ametropie. Graefe Arch Clin Exp Ophthalmol 1934;132:182–223.
2. Stenstrom S. Investigation of the variation and the correlation of the optical elements of human eyes. Am J Optom Arch Am Acad Optom 1948;25:496–504.
3. Benjamin B, Davey JB, Sheridan M, Sorsby A, Tanner JM. Emmetropia and its aberrations; a study in the correlation of the optical components of the eye. Spec Rep Ser Med Res Counc (G B) 1957;11:1–69.
4. Sorsby A, Sheridan M, Leary GA, Benjamin B. Vision, visual acuity, and ocular refraction of young men: findings in a sample of 1,033 subjects. Br Med J 1960;5183:1394–8.
5. Sorsby A, Benjamin B, Bennett AG. Steiger on refraction: a reappraisal. Br J Ophthalmol 1981;65:805–11.
6. Duke-Elder S, Abrams D. The Nature of Refractive Errors. London, UK: Henry Kimpton; 1970.
7. van Alphen GW. On emmetropia and ametropia. Opt Acta (Lond) 1961;142(Suppl):1–92.
8. Attebo K, Ivers RQ, Mitchell P. Refractive errors in an older population: the Blue Mountains Eye Study. Ophthalmology 1999; 106:1066–72.
9. Ojaimi E, Rose KA, Morgan IG, Smith W, Martin FJ, Kifley A, Robaei D, Mitchell P. Distribution of ocular biometric parameters and refraction in a population-based study of Australian children. Invest Ophthalmol Vis Sci 2005;46:2748–54.
10. Mallen EA, Gammoh Y, Al-Bdour M, Sayegh FN. Refractive error and ocular biometry in Jordanian adults. Ophthalmic Physiol Opt 2005;25:302–9.
11. He M, Huang W, Li Y, Zheng Y, Yin Q, Foster PJ. Refractive error and biometry in older Chinese adults: the Liwan eye study. Invest Ophthalmol Vis Sci 2009;50:5130–6.
12. Pointer JS. A 6-year longitudinal optometric study of the refractive trend in school-aged children. Ophthalmic Physiol Opt 2001; 21:361–7.
13. Flitcroft DI. Is myopia a failure of homeostasis? Exp Eye Res 2013; 114:16–24.
14. Flitcroft DI. Emmetropisation and the aetiology of refractive errors. Eye (Lond) 2014;28:169–79.
15. Rozema JJ, Atchison DA, Tassignon MJ. Statistical eye model for normal eyes. Invest Ophthalmol Vis Sci 2011;52:4525–33.
16. Rozema JJ, Atchison DA, Tassignon MJ. Comparing methods to estimate the human lens power. Invest Ophthalmol Vis Sci 2011; 52:7937–42.
17. Aramberri J, Araiz L, Garcia A, Illarramendi I, Olmos J, Oyanarte I, Romay A, Vigara I. Dual versus single Scheimpflug camera for anterior segment analysis: precision and agreement. J Cataract Refract Surg 2012;38:1934–49.
18. Nasser CK, Singer R, Barkana Y, Zadok D, Avni I, Goldich Y. Repeatability of the Sirius imaging system and agreement with the Pentacam HR. J Refract Surg 2012;28:493–7.
19. Savini G, Carbonelli M, Sbreglia A, Barboni P, Deluigi G, Hoffer KJ. Comparison of anterior segment measurements by 3 Scheimpflug tomographers and 1 Placido corneal topographer. J Cataract Refract Surg 2011;37:1679–85.
20. Wang Q, Savini G, Hoffer KJ, Xu Z, Feng Y, Wen D, Hua Y, Yang F, Pan C, Huang J. A comprehensive assessment of the precision and agreement of anterior corneal power measurements obtained using 8 different devices. PLoS One 2012;7:e45607.
21. Jasvinder S, Khang TF, Sarinder KK, Loo VP, Subrayan V. Agreement analysis of LENSTAR with other techniques of biometry. Eye (Lond) 2011;25:717–24.
22. Salouti R, Nowroozzadeh MH, Zamani M, Ghoreyshi M. Comparison of the ultrasonographic method with 2 partial coherence interferometry methods for intraocular lens power calculation. Optometry 2011;82:140–7.
23. Zhao J, Chen Z, Zhou Z, Ding L, Zhou X. Evaluation of the repeatability of the Lenstar and comparison with two other noncontact biometric devices in myopes. Clin Exp Optom 2013; 96:92–9.
24. Rabbetts RB. Bennett & Rabbetts' Clinical Visual Optics, 4th ed. Edinburgh, UK: Butterworth-Heinemann; 2007.
25. Morgan I, Rose K. How genetic is school myopia? Prog Retin Eye Res 2005;24:1–38.
26. Meng W, Butterworth J, Malecaze F, Calvas P. Axial length of myopia: a review of current research. Ophthalmologica 2011; 225:127–34.
27. AlMahmoud T, Priest D, Munger R, Jackson WB. Correlation between refractive error, corneal power, and thickness in a large population with a wide range of ametropia. Invest Ophthalmol Vis Sci 2011;52:1235–42.
28. Carney LG, Mainstone JC, Henderson BA. Corneal topography and myopia. A cross-sectional study. Invest Ophthalmol Vis Sci 1997; 38:311–20.
29. Fontana ST, Brubaker RF. Volume and depth of the anterior chamber in the normal aging human eye. Arch Ophthalmol 1980; 98:1803–8.
30. Garner LF, Yap M, Scott R. Crystalline lens power in myopia. Optom Vis Sci 1992;69:863–5.

Jos Rozema
Department of Ophthalmology
Antwerp University Hospital
Wilrijkstraat 10
2650 Edegem
Belgium
e-mail: Jos.Rozema@uza.be